The Astrophysical Journal, 700:1884–1895, 2009 August 1 doi:10.1088/0004-637X/700/2/1884

SOLAR VARIABILITY FROM 240 TO 1750 nm IN TERMS OF FACULAE BRIGHTENING AND SUNSPOT DARKENING FROM SCIAMACHY

J. Pagaran, M. Weber, and J. Burrows
Institute of Environmental Physics, University of Bremen, Otto-Hahn-Allee 1 D-28359 Bremen, Germany; pagaran@iup.physik.uni-bremen.de
Received 2008 December 3; accepted 2009 June 1; published 2009 July 17

ABSTRACT

The change of spectral decomposition of the total radiative output on various timescales of solar magnetic activity is of large interest to terrestrial and solar–stellar atmosphere studies. Starting in 2002, SCIAMACHY was the first satellite instrument to observe daily solar spectral irradiance (SSI) continuously from 230 nm (UV) to 1750 nm (near-infrared; near-IR). In order to address the question of how much UV, visible (vis), and IR spectral regions change on 27 day and 11 year timescales, we parameterize short-term SSI variations in terms of faculae brightening (Mg II index) and sunspot darkening (photometric sunspot index) proxies. Although spectral variations above 300 nm are below 1% and, therefore, well below the accuracy of absolute radiometric calibration, relative accuracy for short-term changes is shown to be in the per mill range. This enables us to derive short-term spectral irradiance variations from the UV to the near-IR. During Halloween solar storm in 2003 with a record high sunspot area, we observe a reduction of 0.3% in the near-IR to 0.5% in the vis and near-UV. This is consistent with a 0.4% reduction in total solar irradiance (TSI). Over an entire 11 year solar cycle, SSI variability covering simultaneously the UV, vis, and IR spectral regions have not been directly observed so far. Using variations of solar proxies over solar cycle 23, solar cycle spectral variations have been estimated using scaling factors that best matched short-term variations of SCIAMACHY. In the 300–400 nm region, which strongly contributes to TSI solar cycle change, a contribution of 34% is derived from SCIAMACHY observations, which is lower than the reported values from SUSIM satellite data and the empirical SATIRE model. The total UV contribution (below 400 nm) to TSI solar cycle variations is estimated to be 55%.

Key words: Sun: activity – Sun: faculae, plages – Sun: general – Sun: infrared – Sun: photosphere – sunspots – Sun: UV radiation

Online-only material: color figure

1. INTRODUCTION

Solar spectral irradiance (SSI) variability up to decadal timescales is an important physical quantity in stellar astrophysics (e.g., Hudson 1988) and solar–terrestrial physics (Haigh 2007; Lean 1997). In stellar astrophysics UV, visible (vis), and infrared (IR) spectral irradiances determine properties of the solar-stellar atmosphere, its variability provides clues to magnetic activity on polarity reversal timescales (11 year Schwabe activity cycle for our sun, e.g., Kuhn et al. 1999; Kuhn 2004; Pipin & Kichatinov 2000) and on rotational timescales (Carrington rotation for our sun, e.g., Hempelmann & Donahue 1997; Hempelmann 2002, 2003) as indicated by the evolution and passage of active regions that consist of dark features called sunspots and small numerous bright points called faculae. Both sun's radiative output and particle flux are altered by emerging/evolving and decaying active regions. They modify composition (chemistry) and dynamics (circulation) in the terrestrial atmosphere, therefore, driving Earth's weather and climate system (Lean 1997; Lean & Rind 2001; Schmieder et al. 2004; de Jager 2005; Basu & Pallamraju 2006; Foukal et al. 2006; Haigh 2007). Atmospheric UV absorption by ozone determines the atmospheric heating rates needed by chemistry transport and climate models to describe solar influence on atmospheric chemistry and dynamics (Matthes et al. 2004; Haigh 2007; Nissen et al. 2007).

A detailed summary on solar variability can be found in de Toma et al. (2004), Fröhlich & Lean (2004), and Bonnet (2006). Among various periodicities, the 11 year solar cycle is the most pronounced to affect current terrestrial stratospheric ozone trends (Dhomse et al. 2006; Steinbrecht et al. 2004, 2006). Different satellite platforms have established variations of total solar irradiance, (TSI or "solar constant") to vary between 0.003% and 0.015% in minutes, 0.2% in months, and 0.1% over decades (Lang 2006; Fröhlich & Lean 2004; Foukal 2004; Hufbauer 1991). Below 300 nm spectral measurements and their variation are well established, however, it contributes only about 1% to the total solar irradiance and less than 20% to TSI variation over a 11 year solar cycle (Rottman et al. 2004; Rottman 2006). Most UV satellite instruments also cover the longwave or near-UV region (UVA: 300–400 nm), where solar cycle variations are below the long-term calibration uncertainty of current space measurements (DeLand et al. 2004). Nevertheless, solar cycle variation in the UVA has been measured from satellites, but these measurements show a wide range of variation from 18% (Lean et al. 1997) to 36% (Krivova et al. 2006) as derived from SOLSTICE and SUSIM observations, respectively. Depending on these numbers the total UV contribution (100–400 nm) to TSI solar cycle variations lies somewhere between 30% and 60%. Above 400 nm changes in solar spectral irradiance on 11 year timescales have not been measured so far and are only available from model estimates (Mitchell & Livingston 1991; Unruh et al. 1999; Krivova et al. 2006).

Regular and nearly daily UV spectral solar observations from space are provided since the late 1970s (Floyd et al. 2004). Vis and near-infrared (near-IR) observations have been rather sporadic and a summary of early vis and near-IR solar spectral observations is provided by Thuillier et al. (2004). Regular daily observations in the visible region up

to 800 nm started with GOME in 1995 (Burrows et al. 1999; Weber et al. 1998). Since 2002 SCIAMACHY (Scanning Imaging Absorption Spectrometer for Atmospheric CHartographY) extends daily coverage continuously to 1750 nm and with some gaps up to 2.4μ (Bovensmann et al. 1999; Skupin et al. 2005a, 2005b). Since 2003, SIM (Harder et al. 2005a, 2005b) provides measurements in the vis and near-IR without gaps up to 3μ at a lower spectral resolution than SCIAMACHY. The data record from SCIAMACHY and SIM are not sufficiently long to cover the complete optical range over an entire solar cycle. Expected solar variability per wavelength is well below 1% above 400 nm and are below absolute radiometric calibration accuracy and long-term calibration stability, however, signal-to-noise ratio for SCIAMACHY ($\sim 10^4$) is sufficiently high to reach sensitivity to solar changes in the per mill level, at least for fairly short periods like over several 27 day solar rotation periods; this sensitivity is enhanced in or near onset of solar cycle maximum.

In this paper, we estimate SSI variability due to the 11 year solar cycle for the entire UV–vis–IR spectral range following a similar proxy-based parameterization scheme as described by Lean et al. (1997, 2000, 2005). Their scheme is based on the assumption that SSI variability in the course of a solar cycle is exclusively due to competing influences of two solar surface features: faculae brightening and sunspot darkening. These surface features evolve as magnetic flux changes (Fligge et al. 2000). The magnetic contributions to irradiance variations can be estimated using solar proxies, the Mg II index for faculae brightening, and the photometric sunspot index for sunspot darkening.

After a brief presentation of solar data and proxies in Sections 2 and 3, we describe in Section 4 how SCIAMACHY measurements are carefully selected and how a simple irradiance model, which we later simply refer to as the SCIA proxy model, is fitted to derive the spectral dependence of scaling factors for faculae brightening and sunspot darkening parameters. In Section 5, results from fitting our simple empirical model across the UV/vis and near-IR spectral range are discussed. The solar cycle change of SSI is obtained by multiplying the derived parameters to typical change of proxies between solar minimum and solar maximum (Section 6). Our results are compared with SUSIM satellite observations and the empirical solar model SATIRE from Krivova et al. (2006) in the 240–400 nm region during solar cycle 23. Section 7 provides a summary and conclusions.

2. SCIAMACHY SOLAR MEASUREMENTS

SCIAMACHY, which stands for Scanning Imaging Absorption Spectrometer for Atmospheric Chartography, is a UV, vis, and near-IR double monochromator for trace gas observations in our terrestrial atmosphere (Bovensmann et al. 1999; Slijkhuis 2005; Gottwald et al. 2006). It covers the wavelength region from 212 nm to 2386 nm (2.4μ) in eight spectral channels with some gaps in the near-IR where atmospheric water vapor saturates (1.8–1.9μ and 2.0–2.2μ). The spectral resolution is moderately high (with respect to most space borne sensors) varying from 0.2μ (Channel 1: 212–334 nm) to 1.5μ (Channel 6: 971–1773 nm). Incoming light is pre-dispersed by a prism and further dispersed by holographic diffraction gratings in each of the eight channels. For the five short wavelength channels (up to 1063 nm), EG&G Reticon diode arrays with 1024 detector pixels are used, in the remaining three near-IR channels InGaAs detectors with 1024 detector pixels each (Manufacturer EPITAXX, now owned by JDS Uniphase). For optimum detector performance, a mixture of 53% Indium and 47% Gallium has been epitaxially grown on the InP substrate. For longer wavelengths (detector pixels 794–1024 in Channel 6 and all pixels in Channels 7–8) a mixture with a higher Indium content was selected, however, this mixture has a reduced performance with regard to dark current noise and number of usable detector pixels (Lichtenberg et al. 2006). The detectors are cooled with a passive radiative cooler, Channels 1–6 down to about 200 K to 224 K, lower temperatures (~150 K) are provided for Channel 7 and 8 detectors. Ice contamination on the near-IR detectors in space strongly reduced optical throughput. After repeated decontamination periods, where the detector was heated, the throughput had improved but residual ice contaminations remained. This is the main reason the spectral region above 1.6μ has not been used in this study. Dead or bad pixels, mostly in the near-IR channels, have been excluded as well.

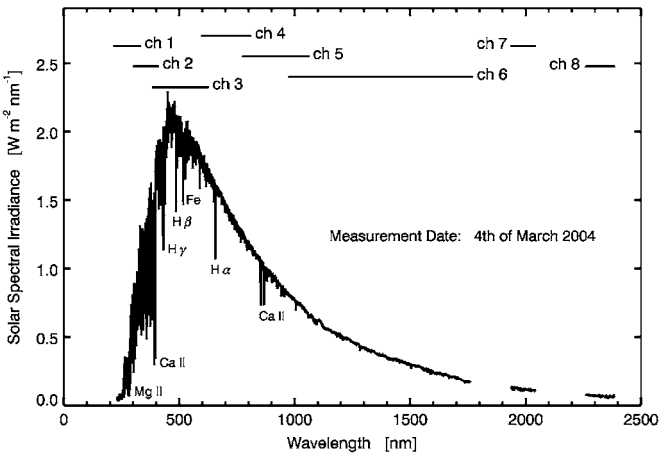

Figure 1. SCIAMACHY solar spectral irradiance measured on 2004 March 4. The eight channels (Channels 1 to 8) and their respective spectral coverage (horizontal solid lines) are indicated above the spectrum. Between Channels 6, 7, and 8 are gaps due to terrestrial atmospheric water vapor. Some of the major Fraunhofer lines are labeled.

The primary purpose of direct solar measurements is to sun-normalize the backscattered light from the terrestrial atmosphere, which to first order does not require absolute radiometric calibration. Different atmospheric viewing geometries are available for SCIAMACHY including nadir viewing, limb, and solar (lunar) occultation (Bovensmann et al. 1999). For each viewing geometry different combinations of scan mirrors (elevation and azimuth scan mirrors) and diffusers (mounted on the back of each scan mirror) are used to observe the sun. Only one light path is absolute radiometrically calibrated and provides solar spectral irradiance in physical units from the full solar disc. This path involves the Azimuth Scan Mirror (ASM) and the diffuser mounted on the back of the Elevation Scan Mirror (ESM diffuser). The diffuser scatters solar light into a diffuse beam to illuminate the entrance slits evenly. Absolute radiometric calibration has been carried out pre-flight using a combination of spectralon/NASA sphere and FEL lamps. ESM diffuser solar measurements are carried out in most cases once a day. A measurement sequence lasts about 50 s from which a mean solar spectrum is derived. A mean ESM diffuser solar spectrum recorded with SCIAMACHY on 2004 March 4 is shown in Figure 1. About 98% of the TSI (total solar irradiance, solar constant) is covered by SCIAMACHY. Wavelengths are calibrated using atomic lines from a Pt/Ne/Cr/Ar lamp that are regularly measured in-flight (Bovensmann et al. 1999; Gottwald et al. 2006).

Daily solar observations with SCIAMACHY aboard ENVISAT started in 2002 August. Continuous observations were interrupted for short periods for ice decontamination of the near-IR detectors (detector warmings) and during ENVISAT platform or SCIAMACHY instrument anomalies, and for other maintenance activities. These interruptions can cause small artifacts in the solar irradiance timeseries as will be discussed later. No additional absolute radiometric calibrations are performed in-flight, so that degradation from harmful UV space radiation is not corrected. The spectrum shown in Figure 1 has been degradation corrected using white light spectrum (WLS) ratios observed regularly in-flight with SCIAMACHY. Since the WLS is even optically degrading faster than the solar data, WLS corrections were not used in our analysis reported here. During night time of each orbit, dark current and straylight measurements are performed and used to correct the detector signal (Lichtenberg et al. 2006). Other important calibrations are the memory effect (residual signal from the previous detector readout, UV–vis channels only), pixel-to-pixel gain, and nonlinearity effect of the near-IR detectors. Most of these calibration parameters were determined pre-flight on ground (Lichtenberg et al. 2006).

In Skupin et al. (2005b), solar irradiance measured from SCIAMACHY have been compared to solar data from SIM (Harder et al. 2005a, 2005b) and SOLSPEC (Thuillier et al. 2004). The three spectra agree to within 3% for the entire wavelength range, larger deviations of up to 5% were found below 300 nm (Skupin et al. 2005a, 2005b). Except for Channels 7 and 8, no significant spectral degradation was observed until 2004. From SCIAMACHY solar observations, the Mg II core-to-wing ratio at 280 nm has been derived (Skupin et al. 2005b). SCIAMACHY measurements complement the GOME timeseries starting in 1995 (Weber 1999; Viereck et al. 2004). In this study, the GOME/SCIAMACHY Mg II index together with multiple satellite data from Viereck et al. (2004) were combined to serve as a faculae brightening proxy.

3. SOLAR PROXIES: FACULAE BRIGHTENING AND SUNSPOT DARKENING

Faculae are enhanced emissions from bright magnetic field elements in the chromosphere and are usually monitored using faculae indices such as chromospheric flux ratios, e.g. the Mg II (280 nm) or Ca II (394 nm) core-to-wing ratios (Weber et al. 1998). It has been shown that UV solar irradiance variability correlate very well with Mg II index changes down to about 30 nm (He II; DeLand & Cebula 1993; Weber 1999; Viereck et al. 2001). The Mg II core-to-wing ratio is obtained by dividing narrow Mg II h and k core emissions by nearby continuum wing fluxes. Core emissions of the Mg II doublet are formed in the chromosphere, while the continuum originates in the photosphere. Calculation of a core-to-wing ratio makes the index largely independent of any instrumental drifts and optical degradation (Heath & Schlesinger 1986). SCIAMACHY Mg II data have been combined with data from GOME (Weber et al. 1998; Weber 1999; Skupin et al. 2005b) and other satellite data (SUSIM, and SBUVs) to update the multiple satellite composite proxy from Viereck et al. (2004). This updated Mg II composite has been corrected to take into account the anomalously low solar cycle 24 minimum and has been extended backwards to 1947 using solar F10.7 cm radio flux and other proxies (M. Weber et al. 2009, in preparation). The latter Mg II composite is used here and in subsequent papers (J. Pagaran et al. 2009a, 2009b, 2009c, in preparation). Missing Mg II core-to-wing ratios were calculated using bicubic spline interpolation. The composite Mg II index is shown in Figure 2.

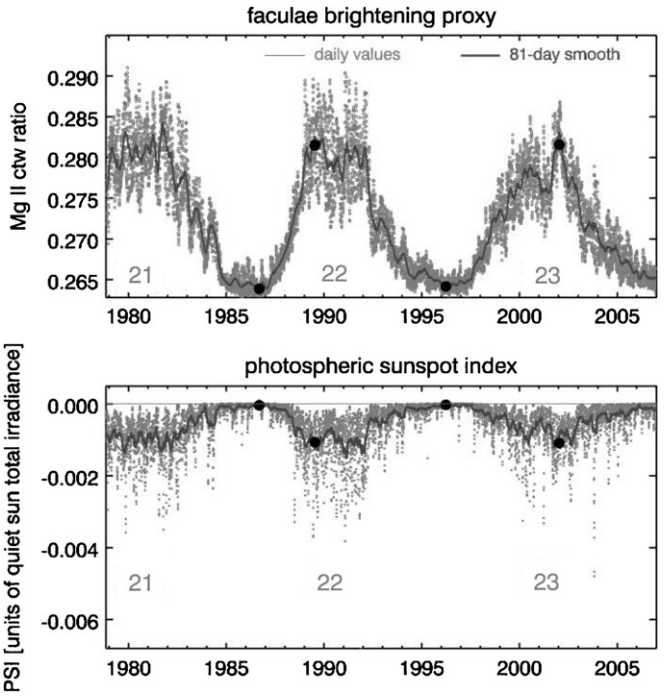

Figure 2. Mg II core-to-wing ratio (top panel) and photometric sunspot index (PSI, bottom panel). Daily values (points) and an 81 day smooth (solid line) are shown as well as values for extrema of the last two 11 year solar cycles. Dates (filled circles) of solar cycle minima and maxima are based on peaks and troughs of the 81 day boxcar-smoothed Mg II index.

Similar to TSI, solar spectral irradiance variations in the optical spectral range varies with changes in faculae brightenings, sun spots, and their distribution on the solar discs (Lean et al. 1997; Fröhlich & Lean 2004; Lean et al. 2005). Their changes are mostly related to magnetic surface activity (Krivova et al. 2003). The effect of sunspot darkening is usually described by the photometric sunspot index (Lean et al. 1997, and references therein), which takes into account area, hemispheric location, and contrast of sunspots as well as center-to-limb variations. Here, we use an updated and homogenized composite photometric sunspot index (PSI) based upon telescope observations from different sites (Balmaceda et al. 2005, 2009). The PSI timeseries is shown along with the Mg II index in Figure 2. Apart from the 11 year solar cycle signature, high-frequency changes with a periodicity of about 27 days related to solar rotations are evident in both timeseries.

Both proxies are anticorrelated, with a correlation coefficient of $\rho(P_a, P_b) = -0.75$ over the nearly 30 year time period (1978–2006). Hereafter, we denote $P_a(t)$ and $P_b(t)$ to interchangeably refer to Mg II and PSI indices, respectively. In the SCIA proxy spectral irradiance model (next section) we alternatively use orthogonalized solar proxies by replacing the PSI term with the sunspot darkening excess. Without modifying or detrending the original proxies, this excess is obtained through a simple linear regression,

$$P_b(t) = A\,P_a(t) + B, \tag{1}$$

and by subtracting the scaled Mg II from PSI. The difference, which is given by

$$P_{b'}(t) = P_b(t) - A\,P_a(t), \tag{2}$$

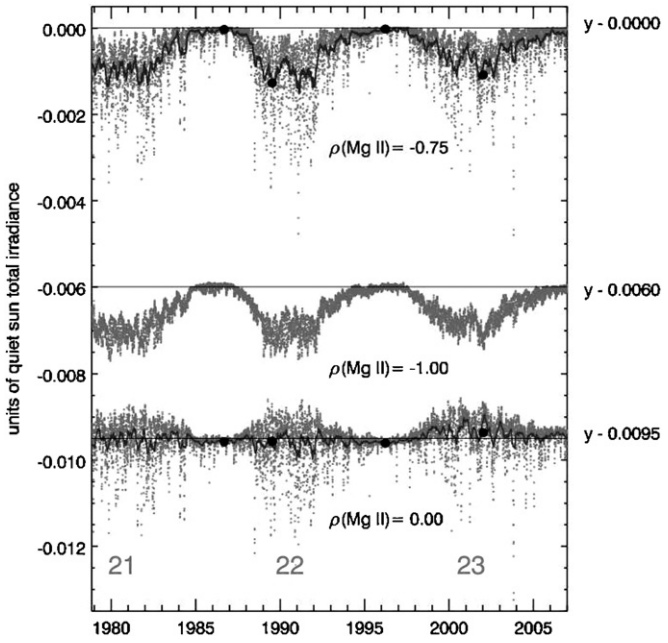

Figure 3. Decomposition of PSI index. Top panel: PSI index, middle panel: Mg II index (top panel of Figure 2) linearly scaled to match the PSI index. Bottom panel: sunspot darkening excess obtained by subtracting the middle panel from PSI timeseries. Filled circles indicate typical proxy values for solar cycle extrema of last two solar cycles as defined by dates from the 81 day boxcar-smoothed Mg II index.

is called photometric sunspot excess (PSE) and is plotted in the bottom panel of Figure 3. The PSE proxy does not correlate with Mg II. Our orthogonalization procedure closely resembles the sunspot subtraction approach described in Lean et al. (1997).

4. DATA ANALYSIS

A simple irradiance model that includes two solar proxies, Mg II and PSI, and additional terms to account for instrumental artifacts (degradation and jumps after decontamination and instrument/platform anomalies) are used here to describe short-term SSI variations. The solar spectral irradiance $I_\lambda(t)$ averaged over a wavelength interval λ can be written as a timeseries as follows:

$$\langle I_\lambda(t)\rangle = a_\lambda P_a(t) + b_\lambda P_b(t) + p_\lambda(t), \quad (3)$$

where $P_a(t)$ and $P_b(t)$ are Mg II index and PSI timeseries, respectively. In the case of using orthogonalized proxies, the symbols (variables and indices a and b) are replaced with primed symbols

$$\langle I_\lambda(t)\rangle = a'_\lambda P_{a'}(t) + b'_\lambda P_{b'}(t) + p_\lambda(t), \quad (4)$$

where $P_{a'}(t) = P_a(t)$ denotes the same Mg II index but $P_{b'}(t)$ denotes the sunspot darkening excess term given in Equation (2).

From Equations (2)–(4), a relationship between primed and unprimed fitting constants a_λ and b_λ can be derived, i.e.,

$$a'_\lambda = a_\lambda - b_\lambda A, \quad (5)$$

$$b'_\lambda = b_\lambda. \quad (6)$$

This means that with one least-squares fit scaling factors for original and orthogonalized proxies are determined. Fitting constants are derived for every wavelength interval λ. They resemble closely faculae and sunspot model intensity spectra in other empirical irradiance models with proxies playing the role of filling factors. See, for example, Fontenla et al. (1999) or Unruh et al. (2000).

In order to distinguish the proxy-based model from actual SCIAMACHY solar data, we call Equation (3) the SCIA proxy model. Either Equation (3) using original proxies or Equation (4) using orthogonalized proxies leads to same modeled quantity $\langle I_\lambda(t)\rangle$. With this model, we quantify short-term variability of SCIAMACHY SSI due to faculae brightening and sunspot darkening, as they evolve/decay and transit across the solar disk. A similar approach has been applied by Lean et al. (1997) to SOLSTICE/UARS data in the spectral region up to 400 nm and by Lean et al. (2005) to SIM data that also include spectral regions above 400 nm. In the absence of SSI measurements above 400 nm, vis–IR variability are usually modeled by constraining the absolute magnitude of the integral of solar spectra over a wide wavelength range to agree with actual bolometric observations of TSI.

The last term, $p_\lambda(t)$, is a short-hand notation for $p_\lambda(t) \equiv \sum_{j=0}^{n} p_{\lambda j}(t)$, where index j indicates a time segment with $t_j < t < t_{j+1}$, for which a polynomial is fitted. Outside this time segment $p_{\lambda j}(t)$ is zero. n is the number of time segments defined for a given irradiance timeseries. $p_{\lambda j}(t)$ is a low-order polynomial that is added to describe the long-term changes of the instrument (degradation) or any other irregularities in the data. The SCIAMACHY irradiance timeseries is split into different time segments. For each time segment, which represents for instance a period between two decontamination phases without any other irregularities, separate polynomials are fitted as will be explained below in more details. This analysis is performed for two different SCIAMACHY observation periods, the first only covering the year 2003 and the second spanning years 2003 and 2004. In 2003 November, the Halloween solar event produced record high sunspot areas that show a clear signal in SSI throughout the entire SCIAMACHY spectral region up to 1.7μ. The use of different periods, 2003 (one year) and 2003–2004 (two years) shall provide insight into the robustness of our results. In both years number of instrument/platform anomalies, decontaminations, and interruptions due to maintenance operations were at their minimum and, on the other hand, optical degradation was less advanced (within one to two years after launch). For 2003, 324 daily SCIAMACHY measurements are available, in 2004 a total of 353 measurements.

The wavelength range (240–1750 nm) has been divided into 143 intervals, each 10 nm wide and the SSI has been averaged over these intervals as follows:

$$\langle I_\lambda(t)\rangle = \frac{\sum_{j=0}^{N} \frac{1}{2}[I(\lambda_k) + I(\lambda_{k+1})] \cdot (\lambda_{k+1} - \lambda_k)}{\lambda_f - \lambda_i} \quad (7)$$

with $(\lambda_f - \lambda_i) \approx 10$ nm to produce a SSI timeseries $\langle I_\lambda(t)\rangle$ for every wavelength interval λ. Here, k is a detector pixel index excluding bad pixels. The choice of 10 nm wavelength bins aims at increasing the signal-to-noise ratio. Because SCIAMACHY has a moderately high spectral resolution, SCIAMACHY can easily be degraded to any desired resolution, for instance, to SIM's resolution as shown later in Section 5. Dispersion is determined by a polynomial to Pt/Ne/Cr/Ar lamp line detector positions.

In the following, we describe a set of selection criteria we have applied in order to decide: which data from SCIAMACHY observations to discard; which ones to retain in our analysis; and

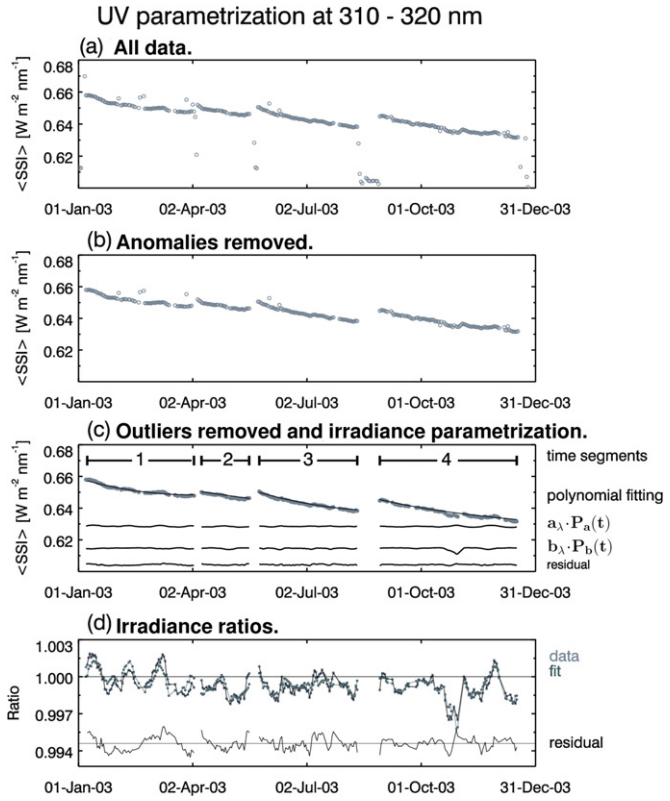

Figure 4. Step-by-step filtering of SCIAMACHY irradiance data and parameterization of short-term SSI variations in the 310–320 nm interval. Shown is the SCIAMACHY timeseries during 2003. Top panel (a): Calibrated SCIAMACHY irradiance timeseries without filtering and without degradation correction. Second panel (b): SCIAMACHY irradiance with data during instrument anomalies and few days before and after removed. Third panel (c): SCIAMACHY timeseries with additional outliers removed by visual inspection. Selected time segments numbered 1–4 are indicated for which separate polynomials are fitted for degradation correction. Solid lines show individual polynomials by fitting Equation (3) to SCIAMACHY irradiances. Bottom lines show facular brightening and sunspot darkening contributions and fit residuals. Bottom panel (d) shows data and fit results as irradiance ratios (solar irradiance divided by the retrieved polynomial). Fit residuals are shifted for clarity.

how to select an optimum polynomial degree in $p_{\lambda j}(t)$. Figure 4 shows a SCIAMACHY irradiance timeseries in the 310–320 nm window. The top panel shows the unfiltered timeseries of the ESM diffuser solar data. Several outliers and discrete jumps between different time segments are visible and are related to instrument or satellite platform anomalies.

The selection of usable data is shown step-by-step in the lower panels. In the first step, periods of known instrument anomalies or satellite/platform maintenance periods including a few days before and after such events are removed from the timeseries (second panel in Figure 4). These anomalies indicate the boundaries of individual time segments, for which separate polynomials in the fitting procedure are applied. There are still some outliers remaining that are then removed by visual inspection (third panel). Time segments that contain less than 10 data points have also been removed since separation between solar proxy terms and polynomial is rather difficult. If there are negligible jumps before and after an anomaly, two time segments are joined and fitted with one polynomial. Timeseries (years 2003–2004 or year 2003) in each wavelength interval are fitted to obtain a_λ and b_λ, and polynomial coefficients of individual time segments. For each wavelength bin the time segments may change. The third panel of Figure 4 shows model fit results by applying Equation (3) to the filtered timeseries. The individual solar proxy contribution as well as polynomials for each time segment are shown. The bottom panel shows fit residuals (shifted for clarity), which are below ±1.5 per mill in the 310–320 nm wavelength bin. It also shows data and fit results as irradiance ratios, which are calculated by dividing irradiances by the fitted polynomials. The polynomial degree selected for each time segment is generally on the order of 2–4 and the shorter the time segment, the lower the polynomial degree selected.

The selection of an optimum polynomial degree in $p_{\lambda j}(t)$ follows the following criteria. As much as possible we keep degrees of the separate polynomials assigned to different time segments as low as possible. We choose the polynomial degrees such that the (1) residuals appear piecewise continuous between neighboring time segments (2) residuals lie within about ±1 to ±1.5 ppm, and (3) fitting constants a_λ and b_λ are maximum, i.e., some sort of convergence is reached. To meet these conditions, fit to Equation (3) was repeated with successive changes in the polynomial degrees of each time segment.

5. RESULTS

On parameterization of SCIAMACHY irradiances. Figures 5–8 show for different wavelength bins, here 390–400 nm (UV),

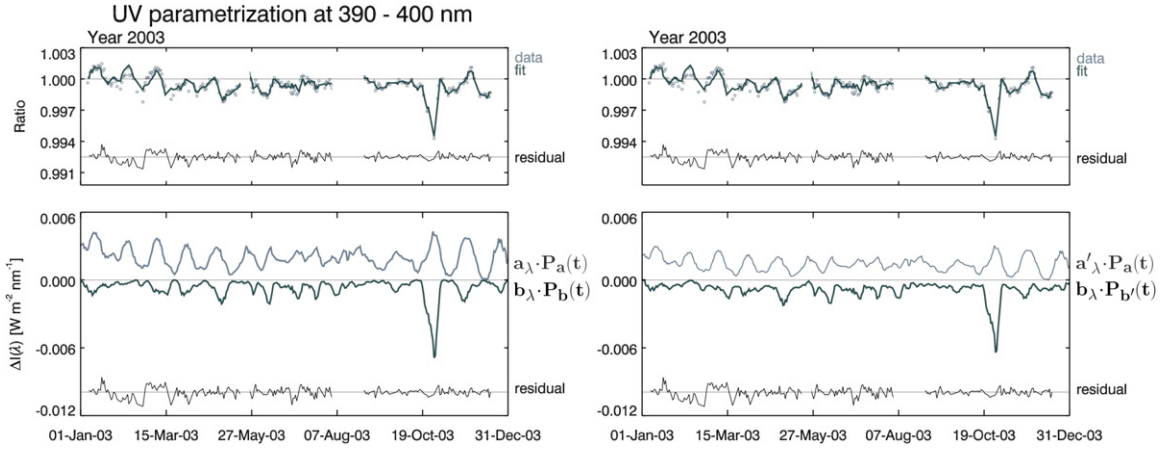

Figure 5. SCIAMACHY irradiance ratio timeseries in the 390–400 nm wavelength bin during 2003. The top panels show SCIAMACHY irradiance ratios (symbols) and model fits (solid line). The fit residuals are shown at the bottom. The bottom panels show facular brightening, $a_\lambda\, P_{\mathrm{Mg\,II}}(t)$, and sunspot darkening, $b_\lambda\, P_{\mathrm{PSI}}(t)$ contributions, and fit residuals in units of W m^{-2} nm. The left panels show fit results using original proxies and the right panels using orthogonalized proxies, which are identical (see the main text).

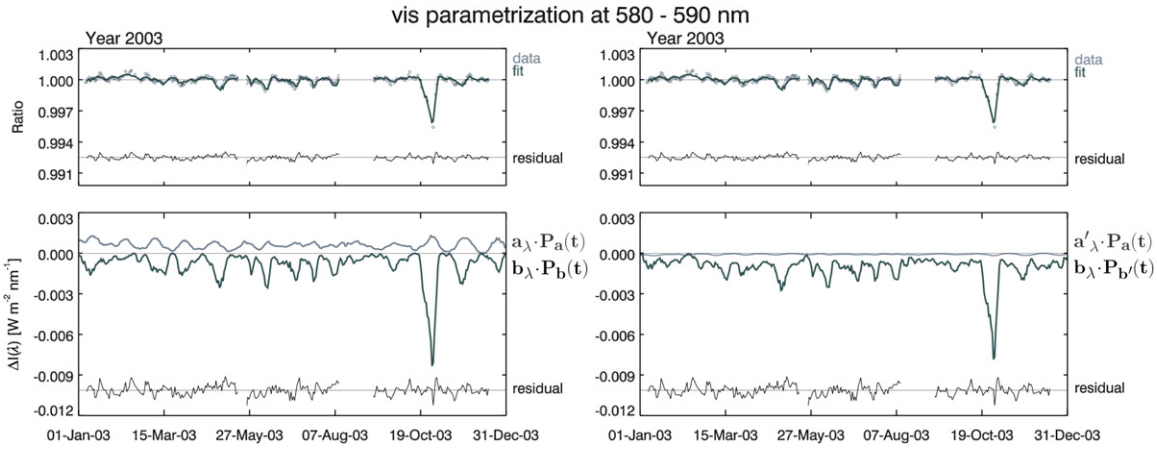

Figure 6. Same as Figure 5 but for 580–590 nm wavelength bin.

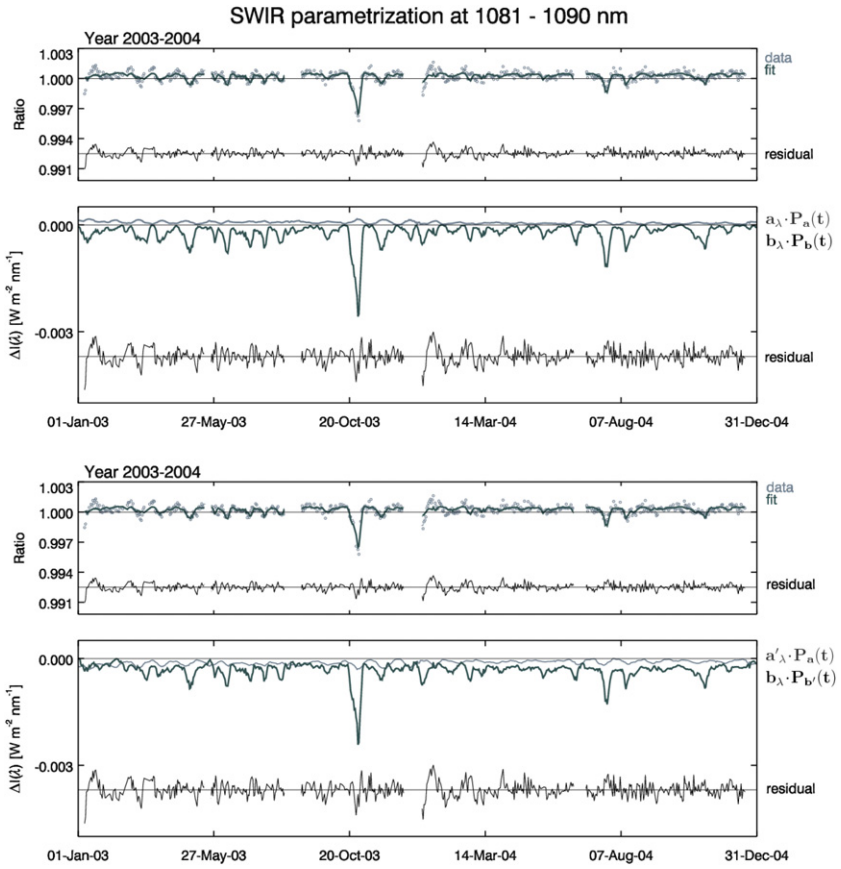

Figure 7. SCIAMACHY irradiance ratio timeseries in the 1080–1090 nm wavelength bin during the two-year period 2003–2004. For more details see Figure 4. Top two panels: modeled and observed irradiance ratios (first panel) and facular brightening and sunspot darkening contributions in units of W m^{-2} nm^{-1} (second panel). The bottom two panels show the same but using fit results with orthogonalized solar proxies.

580–590 nm (vis), 1080–1090 nm, and 1550–1560 nm (both near-IR) results from fitting Equation (3) to the filtered SCIAMACHY irradiance timeseries. In the near-UV (310–320 nm, 390–400 nm, Figures 4 and 5, respectively) contributions from dark sunspots as well as bright faculae are evident. The 390–400 nm band is the region of the Ca II H&K doublet with the second strongest chromospheric emission core after Mg II h&k (280 nm) in the near-UV spectral range (Weber et al. 1998). With a coarse 10 nm wavelength bin size used here these emission cores are not resolved, but at their native spectral resolution the Mg II chromospheric emission cores are barely visible for GOME and SCIAMACHY (Weber et al. 1998; Skupin et al. 2005b). The Halloween event in 2003 indicates a strong reduction of intensity on the order of 0.5% in the near-UV. The right panels of Figures 5 and 6 illustrate the use of Equation (5) to model irradiance timeseries with sunspot darkening excess (orthogonalized sunspot proxy, PSE index) instead of the PSI index. In the near-UV region, differences between original and orthogonalized proxies are not easily detectable, but in the visible region (580–590 nm) the faculae brightening term becomes nearly zero using sunspot darkening excess.

Figures 7 and 8 show fitting results for two near-IR wavelength intervals, 1081–1090 nm and 1550–1560 nm, respectively. The former interval contains the He I 1083 nm absorption

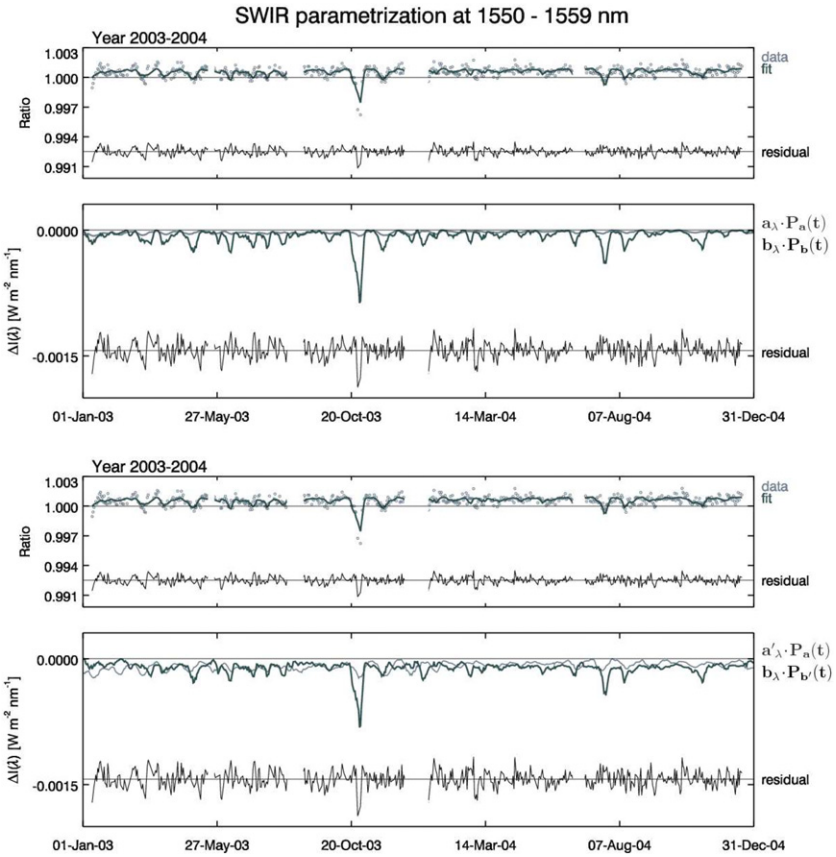

Figure 8. Same as Figure 7 but for 1550–1560 nm wavelength bin.

line originating from the chromosphere (Brajša et al. 1996). The latter interval is in the region of the H^- opacity minimum, where radiation escapes at deeper levels within the photosphere. Here, the dominant contribution is from sunspot darkening. During the Halloween event in 2003, solar near-IR intensity was reduced by 0.3% (-0.003 W m^{-2} nm^{-1} at 1085 nm and -0.0015 W m^{-2} nm^{-1} at 1555 nm). Without the Halloween event near-IR irradiance variations observed by SCIAMACHY are close to noise level (residuals). In the 1550–1560 nm interval (Figure 8), intensity change during the Halloween event is underestimated by our simple model (-0.2% reduction). Between 1400 and 1600 nm the faculae brightening term shows negative values meaning that during high solar activity this spectral region becomes darker. This is consistent with observed dark faculae representing a layer of hot plasma that is optically thick if observed in the vis but optically thin in IR (Foukal et al. 1988, 1989; Moran et al. 1992). The negative contribution arising from the dark faculae reproduces and confirms results from SIM as recently reported by Harder et al. (2008, 2009), contrary to a previous report (based also on SIM data) by Fontenla et al. (2004). This negative contribution is explicitly shown in Figure 10 of Unruh et al. (2008) and suggested in Figure 2 of Unruh et al. (2000). Like our SCIA proxy model, the SATIRE model also underestimated observations near 1550 nm, while good agreement was found at 1060 nm.

Table 1 summarizes correlation coefficients between modeled and observed irradiance ratio timeseries for selected wavelength bins as shown in Figures 5–8. In the UV and vis spectral region correlations are close to 0.9 and lower in the near-IR. The near-IR changes other than during the Halloween solar storm 2003 are close to the noise limit which explains the lower correlation of about 0.8 (fit only in 2003) and 0.7 (fit in 2003–2004).

On derived faculae and sunspot fitting parameters. In Figure 9, fitting parameters for the faculae brightening, a_λ, and sunspot darkening, b_λ, are shown for 10 nm wavelength bins from 240 nm to 1750 nm including 2σ error. Results are shown here from the fit of the one year (2003, filled upright triangles) and two year periods (2003–2004, empty circle line) as well as for original (top two panels) and orthogonalized (bottom panel) proxies. Parameters derived from 2003 and 2003–2004 agree very well with one another. For the validation of our model (see below) we use the parameter derived from the years 2003–2004 being the most robust among the two.

Above about 400 nm the faculae brightening term using orthogonalized proxies drops to nearly zero or slightly negative values right at the long wavelength boundary of the UV spectral region. This means sunspot darkening becomes the dominant solar activity contribution to vis and near-IR irradiance changes. When using original proxies in the SCIA proxy model fits, the faculae brightening term does not show such a sharp transition and remains positive except in the near-IR between 1400 and 1600 nm, the region associated with the dark faculae. In the 800–900 nm interval, a dip in faculae brightening is clearly seen. This dip may be related to reduced optical sensitivity of Al surfaced mirrors (J. Harder 2007, private communication).

We discarded the 975–1070 nm interval (as shown by the gray shaded area) because it is near the boundary of both Channels 5 (high-wavelength end) and 6 (low-wavelength end). Key calibration parameters (polarization sensitivity and radiometric calibration) show steep gradients. Small errors in wavelength calibration error can lead to large shifts in the key parameters and corresponding calibration errors. The

Table 1
Correlation Coefficients between Observed and Modeled Irradiance Ratios and their 1σ Uncertainty for Selected Wavelength Bins

Interval No.	Wavelength Interval [nm]	Spectral Region	No. of Days	Original Proxies	Orthogonalized Proxies
			N	$\rho^2 \pm 1\sigma$	$\rho^2 \pm 1\sigma$
Year 2003 timeseries					
9	310–320	UV	245	0.89339 ± 0.02849	0.89284 ± 0.02863
36	580–590	vis	255	0.92357 ± 0.02036	0.92357 ± 0.02037
83	1081–1090	SWIR	263	0.82536 ± 0.04283	0.82533 ± 0.04284
130	1550–1559	SWIR	252	0.75498 ± 0.05861	0.75495 ± 0.05861
Year 2003–2004 timeseries					
9	310–320	UV	537	0.88732 ± 0.01945	0.88833 ± 0.01929
36	580–590	vis	506	0.87872 ± 0.02151	0.87870 ± 0.02151
83	1081–1090	SWIR	566	0.74332 ± 0.03929	0.74351 ± 0.03926
130	1550–1559	SWIR	542	0.66548 ± 0.04971	0.66573 ± 0.04968

Notes. In the last two columns, the upper and lower limits of uncertainty, which are determined using Fisher's transformation; the larger one of the two is shown here.

wavelength calibration error comes from extrapolation from the last (first) lamp line portions in the corresponding channel.

From 400–1000 nm, the shape of a_λ and a'_λ qualitatively resembles Figures 4 and 5, respectively, of Unruh et al. (2000). A closer look shows that the SCIA proxy model reproduces a dip near 480 nm and a spike near 500 nm. The wavelength dependence follows an inverse wavelength law (faculae contrast measured in the limb). On the other hand, a'_λ shows a rather flat wavelength dependence (faculae contrast observed in the disk center).

As shown in Figure 9, irradiance enhancement due to faculae, irradiance depletions due to sunspots, or their combined contributions as a function of wavelength from 240 to 1750 nm can be computed for any day that has available solar proxy values. Modeled irradiance change and SCIAMACHY observations during the Halloween solar storm 2003, where total sunspot area reached a three decade high, are shown in Figure 10. The shape of the curves (combined faculae and sunspot contributions and SCIAMACHY measurements) is in qualitative agreement with Figure 6 in Lean et al. (2005). Across the near-UV, vis, and near-IR spectral range solar irradiance dropped by 0.3% (near-IR) to 0.5% (near-UV). This is consistent with a drop of about 0.4% in the total solar irradiance.[1] Below 300 nm an irradiance enhancement due to faculae activity was observed reaching +1.3% near 250 nm.

On comparison to SIM data and SRPM model from Fontenla et al. (2004). SCIAMACHY daily irradiance and SCIA proxy model variability can be compared with measurements from SIM at 515 and 1553 nm for one solar rotation in 2003 June (covering overlapping parts of Carrington rotations 2003 and 2004) as presented in Figure 3 of Fontenla et al. (2004). For these comparisons, SCIAMACHY data and the SCIA proxy model were approximately matched to the spectral resolution of SIM by setting $(\lambda_f - \lambda_i)$ in Equation (7) to 7 and 30 nm, respectively (Harder et al. 2005a, 2005b). The comparisons are shown in Figure 11. SIM observations agree well with SCIAMACHY in the vis, however, SCIAMACHY near-IR data are quite noisy as SCIAMACHY residuals, as discussed before, are on the order of 1.5 per mill. Also shown in this figure are SCIA proxy model fit and SRPM+PSPT image model (hereafter simply called SRPM) results (Fontenla et al. 1999, 2004). The SRPM model reconstructs solar irradiance using representative solar atmospheres corresponding to solar surface features such as sunspot umbra, active network, and others and weights their contribution to SSI by their occurrences and location on solar Ca II K PSPT images (Fontenla et al. 2004).

Differences between models and observations indicate some potential deficiencies in models. For instance, quality of solar Ca II K images and lack of a description of penumbras and pores may impact SRPM model results (Fontenla et al. 2004). The SCIA proxy seems to also not adequately describe the irradiance enhancement, suggesting overestimation of sunspot contribution (Fröhlich et al. 1994), particularly in the vis, after the rotation minimum on 2003 June 10. By this time active regions have approached the limb and faculae have become brighter than when they were at disk center, where faculae contrast is normally very small. Although the PSI index accounts for changes in contrast in the penumbrae (Balmaceda et al. 2005, 2009), contrast modification, however, is just a simple approximation (Lean et al. 1997, 2000, 2005).

6. SOLAR CYCLE IRRADIANCE VARIATIONS

The SCIA proxy model allows us to extrapolate observed short-term variations of SCIAMACHY to solar cycle timescales. Below, we briefly consider only solar cycle 23. For more details and consideration of solar cycles 21 and 22 as well, see J. Pagaran et al. (2009b, in preparation). The solar cycle change, however, depends on the definition of solar maximum and minimum dates and respective proxy values during these dates. Here, we define these dates using an 81 day boxcar-smoothed Mg II index timeseries. This allows us to minimize impact from solar rotations. According to this definition, dates for solar minimum and maximum in solar cycle 23 are 1996 March 19 and 2002 January 11, respectively. A similar definition was used in Krivova et al. (2006). Filled circles in Figure 2 indicate PSI and Mg II values for solar maximum and minimum dates as used here to determine irradiance changes in solar cycle 23. Figure 12 shows an update of Figure 11 in Krivova et al. (2006) with the addition of SCIA proxy model results. The SCIA proxy data compare well with recalibrated SUSIM satellite data (Floyd 1999) and the SATIRE empirical model (Krivova et al. 2003) below 400 nm, however, there seems to be a low bias in the SCIA proxy model. The solar cycle changes for SCIA proxy,

[1] See for instance http://www.pmodwrc.ch/pmod.php?topic=tsi/composite/SolarConstant.

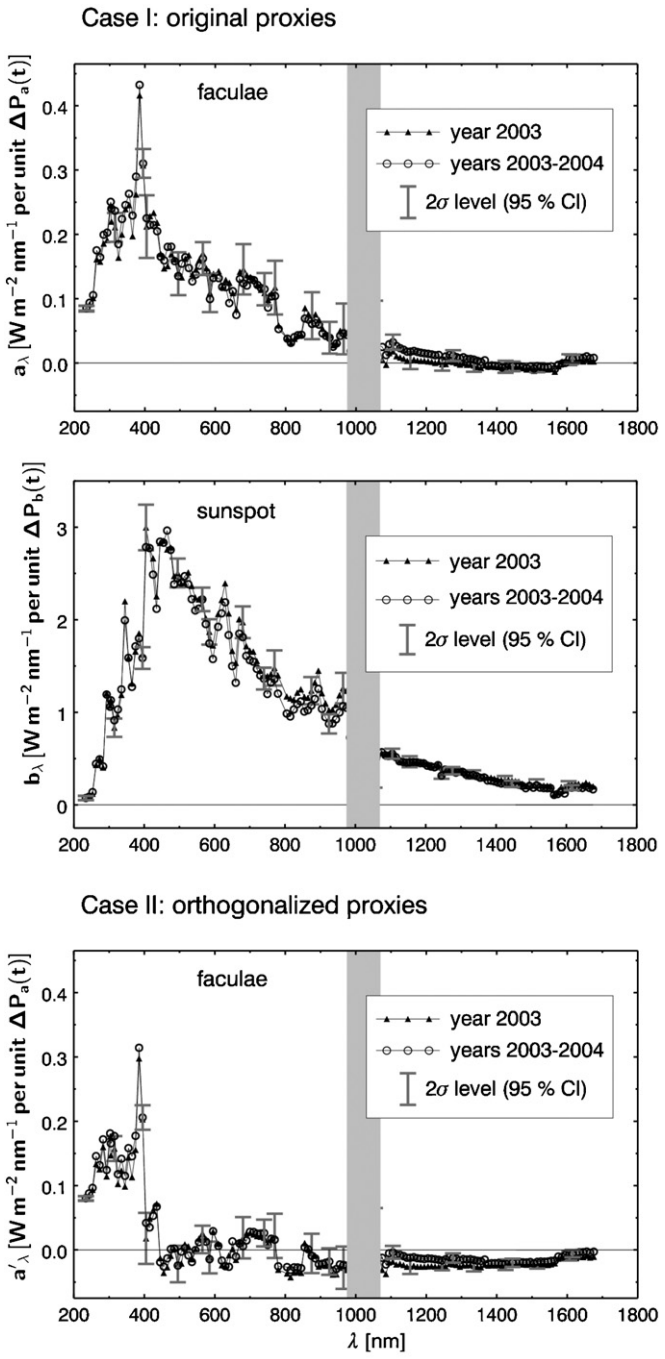

Figure 9. Scaling factors for faculae brightening a_λ and a'_λ in the top and bottom panels, respectively and sunspot darkening b_λ (middle panel) and their respective fitting errors at a 2σ level for both cases when using either original (top two panels) and orthogonalized proxies (bottom two panels). Since b'_λ equals b_λ (see the main text), the middle panel shows the scaling factor for both cases. Each panel depicts two curves as derived from 2003 (one year) and 2003–2004 (two year period). Gray areas indicate discarded wavelength regions (see the main text).

SUSIM, and SATIRE are also summarized in Table 2. This table shows percent spectral contribution in a given wavelength interval to TSI variability ($\Delta F_\lambda/\Delta F_{\rm tot}$). For solar minimum and maximum dates in solar cycle 23, TSI change is 0.134 W m^{-2} after a 81 day boxcar smooth applied to TSI.[2] Overall, our extrapolation of SCIA proxy model to 11 year timescales shows lower SSI variability compared to SUSIM and SATIRE in solar cycle 23 (Figure 12 and Table 2). It is possible that the low bias is due to some low frequency variation in SSI that is not inherent in the solar proxies and gets removed by polynomial terms in the SCIA proxy model. Above 400 nm, extrapolated SSI variability presented in Figure 13 for solar cycle 23 can only be compared qualitatively, for example, with Figure 7 of Unruh et al. (1999) and Figure 2 of Unruh et al. (2000). The overall shape across the whole spectral range agrees qualitatively well. Proper quantitative comparison with SATIRE and Lean et al. models for wavelengths longer than 400 nm will be pursued in another occasion. See J. Pagaran et al. (2009a, 2009b, 2009c, in preparation).

In the SCIA proxy model the wavelength region 240–900 nm contributes 73% to 11 year solar cycle change of TSI, which is lower than the SATIRE model. The SCIA proxy value given for the 800–900 nm wavelength interval may be too low due to reduced spectral responsivity of the Al mirror surface as discussed earlier. The SATIRE model like the SRPM model is an irradiance reconstruction based upon *SOHO* MDI continuum images and magnetograms (Fligge et al. 2000; Krivova et al. 2003; Unruh et al. 2008) from which contributions of faculae and sunspots are derived. In this model, there is one degree of freedom which is selected so that modeled total irradiance matches VIRGO TSI. The low bias in SCIA proxy for solar cycle changes with respect to SATIRE suggests an underestimation of TSI variability contribution.

The SCIA proxy model near-UV estimate of solar cycle variability also has a low bias with respect to SUSIM observations. SUSIM data have been degradation corrected by a simple empirical formula including a Mg II index term to account for natural variability (Floyd 1999; Krivova et al. 2006). Our study as well as Unruh et al. (2008) show that contribution from sunspots is non-negligible in the near-UV as evident in Figure 13. Omitting the sunspot contribution, solar cycle change in the 300–400 nm range for SCIA proxy model increases to 44% per TSI percent change, which is now higher than SUSIM and closer to SATIRE (see Table 2). Figures 3–8, 10, and 13 show that sunspot darkening contributes to irradiance changes at all wavelengths on rotational and decadal timescales. This is in agreement with the study by Unruh et al. (2008), who found significant contributions from both sunspots and faculae in all wavelength regions on rotational timescales.

From the SCIA proxy model the UV contribution between 240 to 400 nm to TSI variability in solar cycle 23 is 47%, which is lower than SUSIM observations (53%) and SATIRE model results (55%) as shown in Table 2. The largest error source in the estimation of solar cycle variations above 300 nm comes from instrument anomaly and degradation corrections that have to be applied to observational data and different approaches for such corrections can impact results, particularly in the spectral region where natural variability is well below the radiometric accuracy.

7. SUMMARY AND CONCLUSIONS

We have parameterized daily UV–vis–IR solar spectral irradiance measurements from SCIAMACHY using appropriate solar proxies describing surface magnetic activity to quantify SSI variability on rotational up to 11 year cycle timescales. Since available solar data in the vis and near-IR from SCIAMACHY (launch in 2002) and SIM (launch in 2003) do not cover a complete solar cycle yet, solar cycle variability derived from

[2] TSI data taken from ftp://ftp.pmodwrc.ch/pub/data/irradiance/composite/DataPlots/ (Fröhlich 2006).

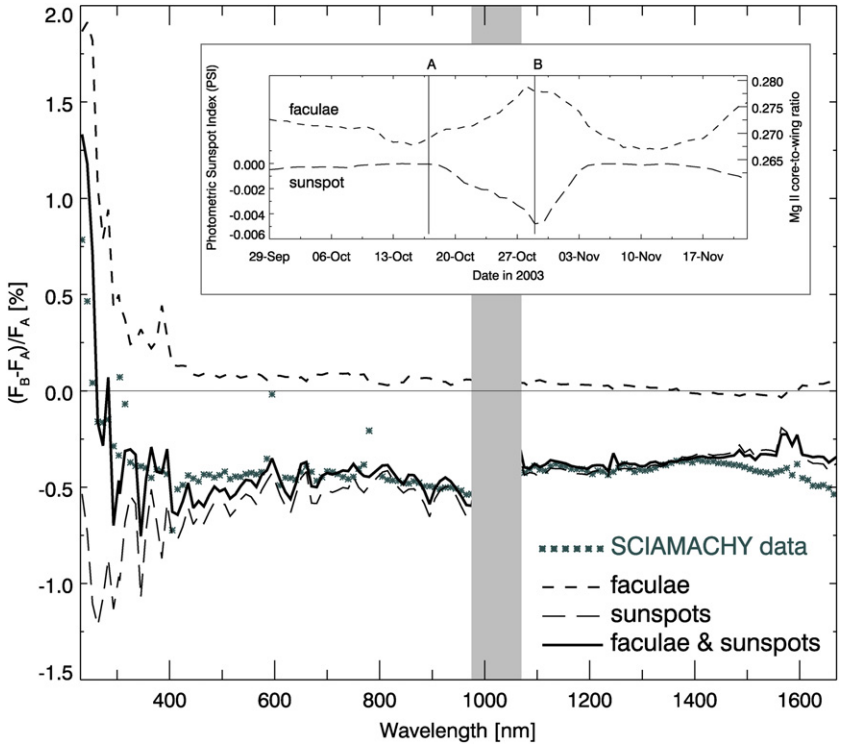

Figure 10. Modeled and observed solar irradiance change from SCIAMACHY during the Halloween storm event in 2003 including facular and sunspot contributions. The inset shows the Mg II and PSI index with labels A and B indicating dates from which irradiance difference was calculated.

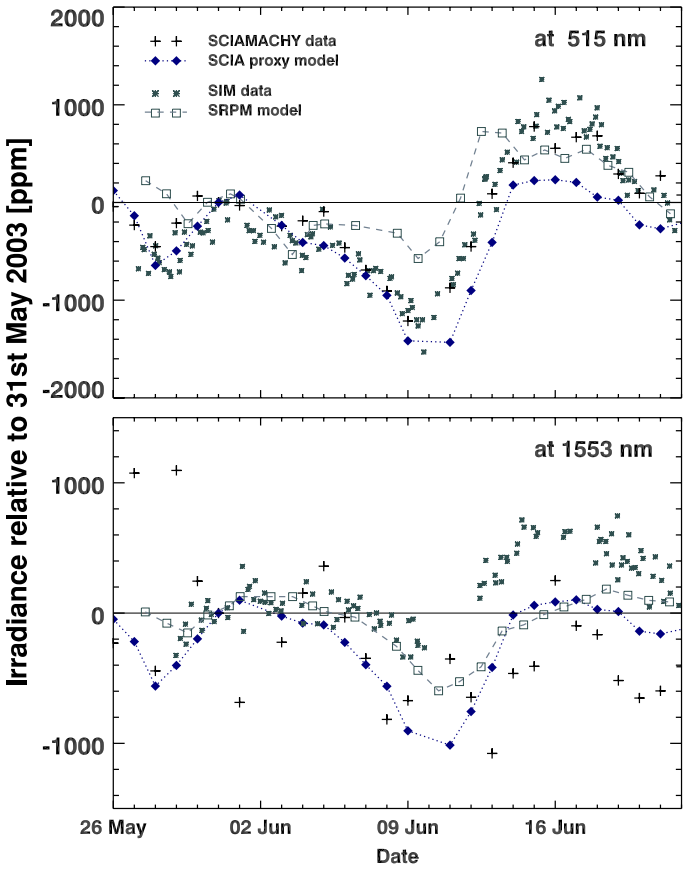

Figure 11. Comparison of SIM and SCIAMACHY irradiance variations with SCIA proxy model and SRPM model from Fontenla et al. (2004). See the main text for more details.

(A color version of this figure is available in the online journal.)

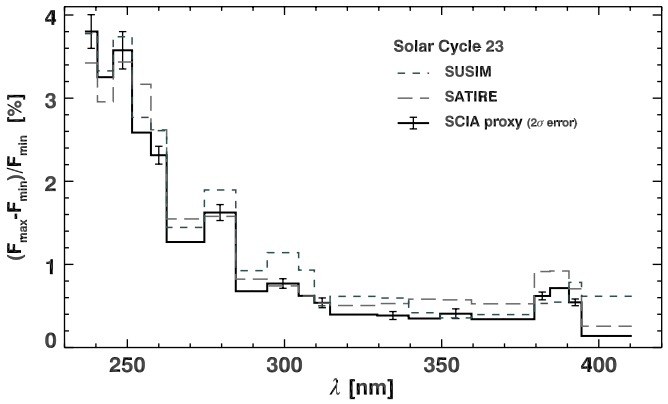

Figure 12. Solar irradiance variations during solar cycle 23 derived from SUSIM and SCIAMACHY satellite observations, and SATIRE model in the near-UV (see also Table 2). SUSIM and SATIRE data are from Krivova et al. (2006).

short-term variations in SCIAMACHY data were extrapolated to solar cycle timescales using solar proxies (Table 2). Variations on solar rotation timescales are of about the same order as solar cycle changes. Solar rotations were modeled using solar proxies accounting for sunspot darkening (PSI index) and faculae brightening (Mg II index). By adding separate polynomials in the SCIA proxy model for each unperturbed observations period without instrument anomalies, instrumental changes were tracked and corrected for (Figure 4).

Scaling parameters for solar proxies were derived from SCIAMACHY observations during the two year period 2003–2004 (Figure 9). Both the PSI and Mg II indices are highly anticorrelated (Figure 2). When using an orthogonalized sunspot darkening proxy, called sunspot darkening excess (PSE) index, faculae brightening contribution sharply drops above 400 nm, therefore, defining a sharp UV boundary toward the vis. Below

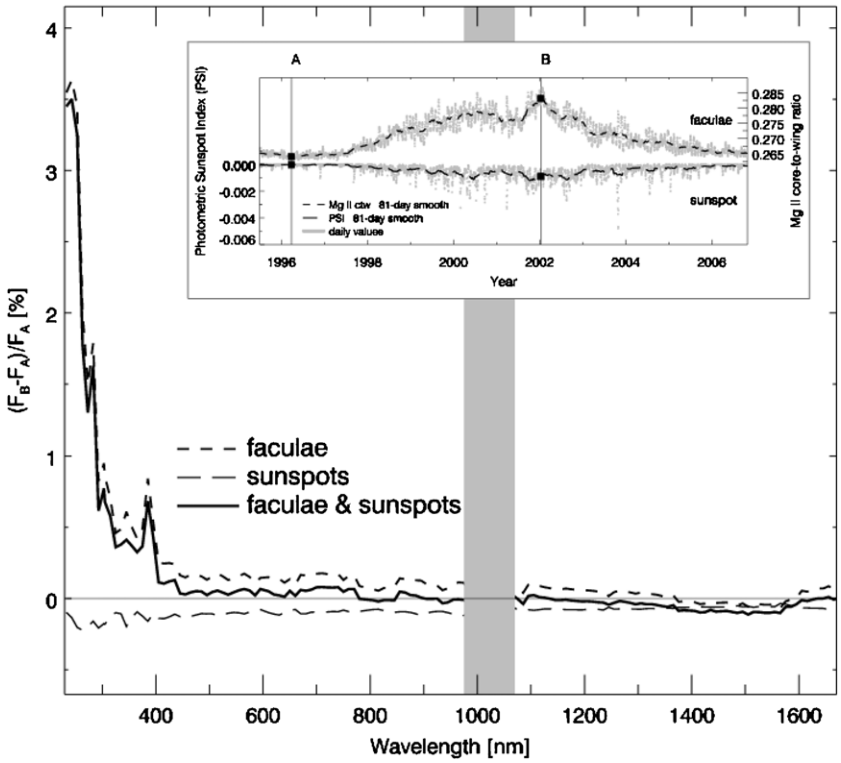

Figure 13. Solar irradiance variations during solar cycle 23 as derived from SCIAMACHY observations and proxy data. Solar maximum and minimum dates were defined by the 81 day boxcar smooth of Mg II index timeseries (inset). Contributions from faculae and sunspots are indicated.

400 nm, the dominant contribution during solar maximum comes from faculae brightening, while the visible regions shows effects from sunspots, but overall changes over a solar cycle are well below 0.5% beyond 300 nm and slightly positive (Figure 13). However, during the Halloween solar storm event in 2003 with a record high sunspot area, the solar irradiance dropped by nearly 0.5% from the near-UV (above 280 nm) to the near-IR (Figure 10). Decomposition of SCIAMACHY irradiance timeseries shows the dark faculae effect in the spectral region 1400–1600 nm (near opacity H^- minimum), where both sunspot and faculae contributions are negative (Figures 8, 9, and 13) in agreement with observations from ground indicating a darkening under enhanced solar activity conditions (Foukal et al. 1988, 1989; Moran et al. 1992). Fontenla et al. (2004) have modified their atmospheric models to accommodate enhancement of IR irradiances seen in SIM solar data (Figure 11). While the enhancement may be valid on short-term scales, our linear scaling of our proxy model indicates a reduction in near-IR irradiance under solar maximum condition.

Our SCIA proxy model can be used to reconstruct spectral irradiances any day during satellite era (after 1978). For more details, see J. Pagaran et al. (2009a, in preparation). The spectral irradiance change during recent solar cycle 23 derived from SCIAMACHY observations is shown in Figure 12 for the UV region and in Figure 13 for the entire optical spectral range. The spectral contribution to TSI variability is summarized in Table 2. Overall there is good agreement with estimates from the SATIRE model (Krivova et al. 2006), but a low bias is seen in the SCIA proxy model. The largest uncertainty in the SCIA proxy derived solar cycle changes comes from the degradation and instrument anomaly correction. If one assumes only a faculae contribution to near-UV changes the agreement between SCIA proxy and SUSIM satellite data in the 300–400 nm wavelength interval is quite good.

Table 2
Irradiance Variation between Solar Maximum and Minimum of Solar Cycle 23 in Different Wavelength Intervals

λ [nm]	F_λ/F_{tot} [%]	$\Delta F_\lambda/\Delta F_{tot}$[%]		
		SCIA Proxy Observations	SUSIM	SATIRE Model
240–300	1.0	12.8	14.6	13.1
300–400	6.7	34.2	38.3	41.8
300–350		16.5	18.5	17.1
350–400		17.7	19.8	24.7
400–500	13.6	9.5	...	12.8
500–600	13.5	6.5	...	7.4
600–700	11.6	4.6	...	5.9
700–800	9.3	5.2	...	6.4
800–900	7.4	0.4	...	5.7
1100–1200	3.9	2.9	...	
1200–1300	3.3	1.5	...	
1300–1400	2.8	0.35	...	
1400–1500	2.4	−0.80	...	
1500–1600	2.0	−0.73	...	

Notes. Column (1) lists the wavelength intervals; Column (2) the percent contribution of spectral irradiance interval, F_λ, to TSI, F_{tot}. Columns (3)–(5) are corresponding percentage contributions of spectral irradiance change, ΔF_λ, in each wavelength interval with respect to solar cycle changes in TSI, ΔF_{tot}. In Column (3) are the SCIA proxy results, Columns (4) and (5) for $\lambda \leqslant 900$ nm are the results from the SUSIM and SATIRE models, respectively, both taken from Krivova et al. (2006). The TSI change, ΔF_{tot}, during solar cycle was 0.134 W m^{-2} (see the main text).

The only other solar cycle variation in the 300–400 nm region derived from satellite observations has been reported by Lean et al. (1997) based upon SOLSTICE/UARS satellite data. Their estimate (from solar cycle 22) seems to be much lower than SCIA proxy and SUSIM, although a similar proxy

model was used. The main difference in their model is that the proxy data as well as solar irradiance data were detrended. In this study, proxy data were not detrended, however, use of polynomials as degradation correction has a similar effect as detrending solar irradiances. The linear scaling of solar proxies then projects their trends on the modeled solar cycle spectral irradiance change. From SCIAMACHY observations, the UV contribution to TSI variability is about 55% (about half), which is lower than the estimate of about 63% (nearly two-third) from SATIRE model (Krivova et al. 2006) but higher than the 30% (one-third) contribution derived from SOLSTICE observations (Lean et al. 1997).

As SSI timeseries covering vis and near-IR region have only become recently available with satellite observations from SIM and SCIAMACHY, investigations of solar rotations using the entire spectral range from UV to IR has recently becoming feasible (Fontenla et al. 2004; Harder et al. 2005c; Unruh et al. 2008). Since irradiance changes are very small beyond 400 nm and well below long-term stability of satellite instruments, derivation of reliable irradiance change estimates over an extended period like a solar cycle remains a challenging task.

SCIAMACHY is a collaboration between Germany, the Netherlands, and Belgium. We are indebted to the entire SCIAMACHY team, whose efforts make this analysis possible. We furthermore thank European Space Agency (ESA) and DLR for processing SCIAMACHY data. We thank Natalie Krivova, Max Planck Institute for Solar System Research, Katlenburg-Lindau, for SATIRE data and for homogenized composite PSI data made by Laura Balmaceda (now at University of Valencia, Spain), Linton Floyd, Interferometrics Inc. and Naval Research Laboratory, for providing SUSIM data and Jerry Harder, Laboratory for Atmospheric and Space Physics, University of Colorado, for obtaining data from Fontenla et al. (2004). They and the first two authors (J.P. & M.W.) of this paper are part of the International Space Studies Institute (ISSI) team[3] on spectral solar irradiance, whose meetings and discussions have benefited this study. This work has been supported by the Deutsche Forschungsgemeinschaft (DFG) project SOLOZON[4] (DFG WE 3647/1–1) within the national CAWSES (Climate And Weather of the Sun–Earth System) priority programme.

REFERENCES

Balmaceda, L., Solanki, S. K., & Krivova, N. 2005, Mem. Soc. Astron. Ital., 76, 929
Balmaceda, L., Solanki, S. K., Krivova, N., & Foster, S. 2009, J. Geophys. Res., in press (arXiv:0906.0942)
Basu, S., & Pallamraju, D. 2006, Adv. Space Res., 38, 1781
Bonnet, R.-M. 2006, Space Sci. Rev., 125, 17
Bovensmann, H., et al. 1999, J. Atmos. Sci., 56, 127
Brajša, R., et al. 1996, Sol. Phys., 163, 79
Burrows, J. P., et al. 1999, J. Atmos. Sci., 56, 151
de Jager, C. 2005, Space Sci. Rev., 120, 197
de Toma, G., White, O. R., Chapman, G. A., & Walton, S. R. 2004, Adv. Space Res., 34, 237
DeLand, M. T., & Cebula, R. P. 1993, J. Geophys. Res. 98, 12, 809
DeLand, M. T., Floyd, L. E., Rottman, G. J., & Pap, J. 2004, Adv. Space Res., 34, 243
Dhomse, S., Weber, M., Wohltmann, I., Rex, M., & Burrows, J. P. 2006, Atmos. Chem. Phys., 6, 1165
Fligge, M., Solanki, S. K., & Unruh, Y. C. 2000, A&A, 353, 380
Floyd, L. 1999, Adv. Space Res., 23, 1459
Floyd, L., Tobiska, W. K., & Cebula, R. P. 2004, Adv. Space Res., 29, 1427
Fontenla, J., White, O. R., Fox, P. A., Avrett, E. H., & Kurucz, R. L. 1999, ApJ, 518, 480
Fontenla, J. M., et al. 2004, ApJ, 605, L85
Foukal, P. 2004, Solar Astrophysics (Berlin: Wiley-VCH)
Foukal, P., Fröhlich, C., Spruit, H., & Wigley, T. M. L. 2006, Nature, 443, 161
Foukal, P., Little, R., & Mooney, J. 1988, BAAS, 20, 689
Foukal, P., Little, R., & Mooney, J. 1989, ApJ, 336, L33
Fröhlich, C. 2006, Space Sci. Rev., 125, 53
Fröhlich, C., & Lean, J. 2004, A&AR, 12, 273
Fröhlich, C., Pap, J. M., & Hudson, H. S. 1994, Sol. Phys., 152, 111
Gottwald, M., et al. 2006, SCIAMACHY, Monitoring the Changing Earth's Atmosphere (Oberpfaffenhofen: DLR Institut für Methodik der Fernerkundung (IMF))
Haigh, J. D. 2007, Living Reviews in Solar Physics, 4 http://www.livingreviews.org/lrsp-2007-2
Harder, J. W., Fontenla, J., Lawrence, G., Woods, T., & Rottman, G. 2005b, Sol. Phys., 230, 169
Harder, J. W., Fontenla, J., Pilewskie, P., Richard, E., & Woods, T. 2008, AGU Fall Meeting Abstracts (Washington, DC: AGU), A1630
Harder, J. W., Fontenla, J. M., Pilewskie, P., Richard, E. C., & Woods, T. N. 2009, Geophys. Rev. Lett., 36, 7801
Harder, J. W., Fontenla, J., White, O., Rottman, G., & Woods, T. 2005c, Mem. Soc. Astron. Ital., 76, 735
Harder, J., Lawrence, G., Fontenla, J., Rottman, G., & Woods, T. 2005a, Sol. Phys., 230, 141
Heath, D. F., & Schlesinger, B. M. 1986, J. Geophys. Res., 91, 8672
Hempelmann, A. 2002, A&A, 388, 540
Hempelmann, A. 2003, A&A, 399, 717
Hempelmann, A., & Donahue, R. A. 1997, A&A, 322, 835
Hudson, H. S. 1988, ARA&A, 26, 473
Hufbauer, K. 1991, Exploring the Sun: Solar Science since Galileo (Baltimore, MD: Johns Hopkins Univ. Press)
Krivova, N. A., Solanki, S. K., Fligge, M., & Unruh, Y. C. 2003, A&A, 399, L1
Krivova, N. A., Solanki, S. K., & Floyd, L. 2006, A&A, 452, 631
Kuhn, J. R. 2004, Adv. Space Res., 34, 302
Kuhn, J. R., Lin, H., & Coulter, R. 1999, Adv. Space Res., 24, 185
Lang, K. R. 2006, Sun, Earth and Sky (2nd ed.; Berlin: Springer)
Lean, J. 1997, ARA&A, 35, 33
Lean, J., & Rind, D. 2001, Science, 292, 234
Lean, J., Rottman, G., Harder, J., & Kopp, G. 2000, Geophys. Res. Lett., 27, 2425
Lean, J., Rottman, G., Harder, J., & Kopp, G. 2005, Sol. Phys., 230, 27
Lean, J. L., et al. 1997, J. Geophys. Res., 102, 29939
Lichtenberg, G., et al. 2006, Atmos. Chem. Phys., 6, 5347
Matthes, K., Langematz, U., Gray, L. L., Kodera, K., & Labitzke, K. 2004, J. Geophys. Res., 109, D06101
Mitchell, W. E., & Livingston, W. C. 1991, ApJ, 372, 336
Moran, T., Foukal, P., & Rabin, D. 1992, Sol. Phys., 142, 35
Nissen, K. M., Matthes, K., Langematz, U., & Mayer, B. 2007, Atmos. Chem. Phys., 7, 5391
Pipin, V. V., & Kichatinov, L. L. 2000, Astron. Rep., 44, 771
Rottman, G. 2006, Space Sci. Rev., 125, 39
Rottman, G., Floyd, L., & Viereck, R. 2004, Geophys. Mono., 41, 111
Schmieder, B., et al. 2004, Adv. Space Res., 34, 443
Skupin, J., Weber, M., Noël, S., Bovensmann, H., & Burrows, J. P. 2005b, Mem. Soc. Astron. Italiana, 76, 1038
Skupin, J., et al. 2005a, Adv. Space Res., 35, 370
Slijkhuis, S. 2005, ENVISAT-1 SCIAMACHY Level 0 to 1c Processing, Algorithm Technical Basis Document, Tech. Rep., DLR, ENV-ATB-DLR-SCIA-0041 (Oberpfaffenhofer: DLR)
Steinbrecht, W., Claude, H., & Winkler, P. 2004, J. Geophys. Res., 109, D14305
Steinbrecht, W., et al. 2006, J. Geophys. Res., 111, D10308
Thuillier, G., et al. 2004, Geophys. Mono., 41, 171
Unruh, Y. C., Krivova, N. A., Solanki, S. K., Harder, J. W., & Kopp, G. 2008, A&A, 486, 311
Unruh, Y. C., Solanki, S. K., & Fligge, M. 1999, A&A, 345, 635
Unruh, Y. C., Solanki, S. K., & Fligge, M. 2000, Space Sci. Rev., 94, 145
Viereck, R. A., et al. 2001, Geophys. Res. Lett., 28, 1343
Viereck, R., et al. 2004, Space Weather, 2, S10005
Weber, M. 1999, in ESA-WPP, European Symp. on Atmospheric Measurements from Space, Proc. ESAMS '99 (Noordwijk: ESA), 161, 611 http://www.iup.physik.uni-bremen.de/gome/solar/weber_esams99.pdf
Weber, M., Burrows, J. P., & Cebula, R. P. 1998, Sol. Phys., 177, 63

[3] http://www.issibern.ch/teams/solarspect/
[4] http://www.iap-kborn.de/CAWSES-Projekt-SOLOZON.373.0.html